Structural Similarities between Biogenic Uraninites Produced by Phylogenetically and Metabolically Diverse Bacteria

JONATHAN O. SHARP,*,†,‡ ELEANOR J. SCHOFIELD,§ HARISH VEERAMANI,† ELENA I. SUVOROVA,† DAVID W. KENNEDY,|| MATTHEW J. MARSHALL,|| APURVA MEHTA,§ JOHN R. BARGAR,§ AND RIZLAN BERNIER-LATMANI†

École Polytechnique Fédérale de Lausanne (EPFL), Switzerland, Stanford Synchrotron Radiation Lightsource (SSRL), Menlo Park, CA, and Pacific Northwest National Laboratory (PNNL), Richland, WA

Received April 29, 2009. Revised manuscript received August 12, 2009. Accepted August 25, 2009.

While the product of microbial uranium reduction is often reported to be "UO_2", a comprehensive characterization including stoichiometry and unit cell determination is available for only one *Shewanella* species. Here, we compare the products of batch uranyl reduction by a collection of dissimilatory metal- and sulfate-reducing bacteria of the genera *Shewanella*, *Geobacter*, *Anaeromyxobacter*, and *Desulfovibrio* under similar laboratory conditions. Our results demonstrate that U(VI) bioreduction by this assortment of commonly studied, environmentally relevant bacteria leads to the precipitation of uraninite with an approximate composition of $UO_{2.0}$, regardless of phylogenetic or metabolic diversity. Coupled analyses, including electron microscopy, X-ray absorption spectroscopy, and powder diffraction, confirm that structurally and chemically analogous uraninite solids are produced. These biogenic uraninites have particle diameters of about 2−3 nm and lattice constants consistent with $UO_{2.0}$ and exhibit a high degree of intermediate-range order. Results indicate that phylogenetic and metabolic variability within delta- and gamma-proteobacteria has little effect on biouraninite structure or crystal size under the investigated conditions.

Introduction

Reductive immobilization has been proposed as an in situ remediation strategy in subsurface waters where soluble, oxidized uranium is converted to a comparatively immobile, insoluble species (*1*). Reduction from a valence of six to four can be mediated by a variety of dissimilatory metal- and sulfate-reducing bacteria (DMRB and DSRB) in liquid batch, including strains of the genera *Anaeromyxobacter*, *Geobacter*, *Shewanella*, and *Desulfovibrio (1−5)*. Soil columns amended with DMRB, denitrifying bacteria, or DSRB have confirmed that reductive immobilization can occur in simplified soil systems (*6, 7*), and analogous field-scale pilot biostimulation studies have successfully immobilized uranium in the subsurface (*8, 9*).

The long-term efficacy of such bioreductive remediation strategies is however dependent upon the identity and composition of the reduced uranium species, characteristics that directly govern the chemical and physical stability of the transformed contaminant. Uraninite is generally regarded as a desirable product of bioreduction because of its low solubility under reducing conditions (*10*). However, the composition of environmental uraninite is believed to vary between $UO_{2.0}$ and $UO_{2.25}$ (U_4O_9), with the latter composition generally regarded as being more stable in the environment (*11, 12*). Moreover, while uraninite has been reported to form by direct and indirect biological reductive processes (*13, 14*), it is not clear if the resultant products are truly conserved between different reductive phenomena. Variations in uraninite crystalline structure or surface area could impart different stabilities and resistance to oxidation (*10*); hence, even subtle differences in the form of immobilized uranium resulting from different bacterial communities and remediation measures in the field could affect the environmental stability of sequestered uranium.

Recent investigations have provided a comprehensive structural characterization of nanoparticulate uraninite produced by *Shewanella*, revealing a near-stoichiometric product with a diameter of ∼3 nm (*14−16*). However, *Shewanella* has not been found to be a prevalent DMRB during biostimulation at contaminated sites (*9, 17, 18*). For example, subsurface ethanol amendments enriched populations of DMRB and DSRB at Oak Ridge, TN. Dominant genera were identified as *Ferribacterium*, *Geothrix*, and *Desulfovibrio* and to a lesser degree *Geobacter*, *Anaeromyxobacter*, *Desulfosporosinus*, and *Acidovorax* (*17*). During acetate amendment of a uranium-contaminated site in Rifle, CO, the community dynamically shifted from *Geobacteraceae* family DMRB to *Desulfobacteraceae* family DSRB in regions where bioavailable Fe(III) was consumed (*9, 18*). Thus,

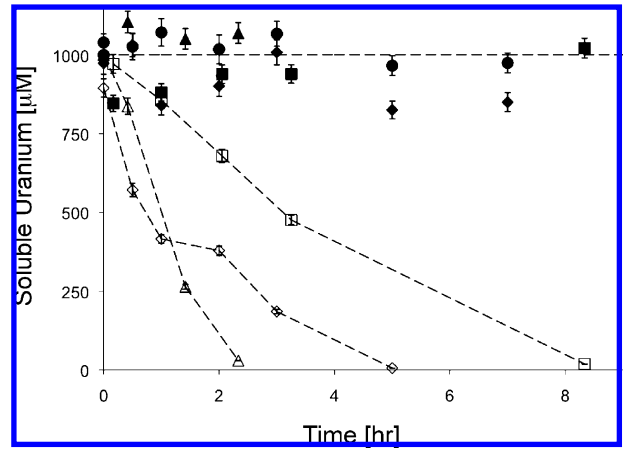

FIGURE 1. Representative removal of 1000 μM uranyl in resting cell assays by active bacterial cultures (open symbols), abiotic, and pasteurized controls (closed symbols), where ■ = pasteurized and □ = active *S. putrefaciens* (200 mg protein/L); ▲ = pasteurized and Δ = active *G. sulfurreducens* (90 mg protein/L); ◆ = pasteurized and ◇ = active *D. vulgaris* (130 mg protein/L); and ● = abiotic control. The T_0 time point for the *Geobacter* set depicts the initial concentration of uranyl added to the system.

* Corresponding author e-mail: jsharp@mines.edu.
† École Polytechnique Fédérale de Lausanne (EPFL).
‡ Present address: Environmental Science and Engineering Division, Colorado School of Mines, Golden, CO.
§ Stanford Synchrotron Radiation Lightsource (SSRL).
|| Pacific Northwest National Laboratory (PNNL).

10.1021/es901281e CCC: $40.75
Published on Web 09/23/2009

TABLE 1. EXAFS Fit Results for Biogenic Uranium Precipitates Produced by Different Bacteria

	U−O_1	U−U_1	U−U_2	U−U_3	U−U_4	SCL[a]
S. oneidensis MR-1						
N	8	5.5 (9)	6	24	12	
R (Å)	2.353 (7)	3.860 (6)	5.46 (2)	6.72 (3)	7.62 (4)	
σ^2 (Å^2)	0.0116 (6)	0.0066 (8)	0.006	0.008	0.004	1.1 (2)
S. putrefaciens CN-32						
N	8	5.7 (8)	6	24	12	
R (Å)	2.352 (6)	3.861 (5)	5.46 (2)	6.71 (3)	7.62 (4)	
σ^2 (Å^2)	0.0104 (5)	0.0058 (6)	0.006	0.008	0.004	1.2 (2)
Shewanella sp. HRCR-2						
N	8	6 (1)	6	24	12	
R (Å)	2.358 (9)	3.862 (9)	5.49 (3)	6.73 (5)	7.61 (9)	
σ^2 (Å^2)	0.0138 (8)	0.009 (1)	0.006	0.008	0.004	0.9 (2)
A. dehalogenans						
N	8	6.1 (9)	6	24	12	
R (Å)	2.352 (7)	3.861 (5)	5.45 (2)	6.71 (3)	7.61 (4)	
σ^2 (Å^2)	0.0124 (6)	0.0067 (7)	0.006	0.008	0.004	1.1 (2)
G. sulfurreducens[b]						
N	8	6.2 (9)	6	24	12	
R (Å)	2.366 (7)	3.865 (5)	5.44 (2)	6.71 (2)	7.61 (3)	
σ^2 (Å^2)	0.0107 (7)	0.0052 (6)	0.006	0.008	0.004	1.5 (2)
D. vulgaris						
N	8	6.4 (9)	6	24	12	
R (Å)	2.356 (7)	3.863 (5)	5.45 (2)	6.72 (2)	7.63 (3)	
σ^2 (Å^2)	0.0107 (7)	0.0054 (6)	0.006	0.008	0.004	1.3 (2)

[a] SCL = Structural coherence length (nm).

[b] An optimal fit for *G. sulfurreducens* (see text) included contributions from surface uranium atoms (39% of U atoms). This was achieved by modifying the EXAFS model to account for bonds to 1 and 2 Fe atoms at 2.98 (1) and 3.16 (2) Å, respectively, fixed σ^2 of 0.005 σ^2, and SCL of the particle set to 2.0. Other parameters are as reported but are scaled to account for the relative contribution of interior atoms (61% of total U).

biogeochemical variability between and within contaminated sites, preferences in remediation strategies, and evolution of community dynamics during a remediation treatment suggest that responsible bacteria could include genetically distinct beta-, delta- and gamma-proteobacteria in addition to phyla such as Acidobacteria and Firmicutes (*9, 17*−*22*). Despite evidence for the involvement of phylogenetically diverse bacteria in environmental U(VI) reduction, there remains a lack of detailed knowledge about the structures of reduced uranium solid phases produced by microorganisms other than *Shewanella*.

In this study, we evaluate the product of batch U(VI) reduction by a suite of commonly studied bacteria. Strains of *Shewanella*, *Geobacter*, *Anaeromyxobacter*, and *Desulfovibrio* were incubated under chemically defined laboratory conditions to investigate variations in reaction products by direct microbial reduction. This is the first comprehensive, interspecies comparison of the crystalline structure of uranium reduction products using coupled transmission electron microscopy (TEM), electron diffraction (ED), X-ray absorption spectroscopy (XAS), and synchrotron powder diffraction (SR-PD). The objective of the study was to identify similarities and differences in biogenically reduced uranium among diverse uranium-reducing bacteria.

Materials and Methods

Cellular Growth and Reduction Assays. U(VI) reduction assays were performed at École Polytechnique Fédérale de Lausanne (EPFL) (*Desulfovibrio vulgaris*, *Geobacter sulfurreducens*, *Shewanella putrefaciens* CN-32, and *S. oneidensis* MR-1) and Pacific Northwest National Laboratory (PNNL) (*Anaeromyxobacter dehalogenans*, *S. oneidensis* MR-1, and *Shewanella* sp. HRCR-2). Axenic cultures were grown at 30 °C and 140 rpm using standard microbiological techniques and strain-specific media for optimal growth as elaborated in the Supporting Information.

After culture-specific growth, late-log phase cells were harvested (10000*g, 5 min), washed twice in a 30 mM sodium bicarbonate buffer (pH 7.0, 4 °C), and suspended in a O_2-free buffer. For uraninite production in analogous media and yields necessary for coupled synchrotron-based analyses, assays were initiated by adding 10 mL of the washed cell suspension (~2−3 × 10^{10} cells/ bottle) to 90 mL of assay mix (final concentration: 30 mM $NaHCO_3$, 10 mM PIPES, e^--donor, 1 mM uranyl acetate, pH 7.0) in anoxic 250 mL serum bottles purged with N_2:CO_2 gas mixture (80:20, vol/vol). Aside from bacteria, the exogenous e^--donor was the sole variable in these assays and was provided as follows: *Geobacter sulfurreducens*, 20 mM acetate; *Desulfovibrio vulgaris* and *Shewanella* spp., 20 mM lactate; *Anaeromyxobacter dehalogenans*, 20 mL H_2 (~815 μmol). Uranium was added after pasteurization of controls (80 °C, 15 min). Reduction assays were incubated at 30 °C with gentle (25 rpm, PNNL) or no agitation (EPFL).

The unrooted phylogenetic tree was assembled using the maximum-likelihood method on ARB (http://www.arb-home.de/) by comparing an aligned 793bp region of 16s rRNA as reported in GenBank.

Sample Monitoring and Processing. At multiple time points, samples were collected in an anoxic atmosphere (COY Laboratory, Grass Lakes, MI) and analyzed for soluble U(VI) remaining in filtrates (<0.2 μm pore size) using a kinetic phosphorescence analyzer (KPA-11A; Chemchek, Richland, WA). After a stationary overnight incubation, the precipitate was collected under anoxic conditions, washed in a 100 mM

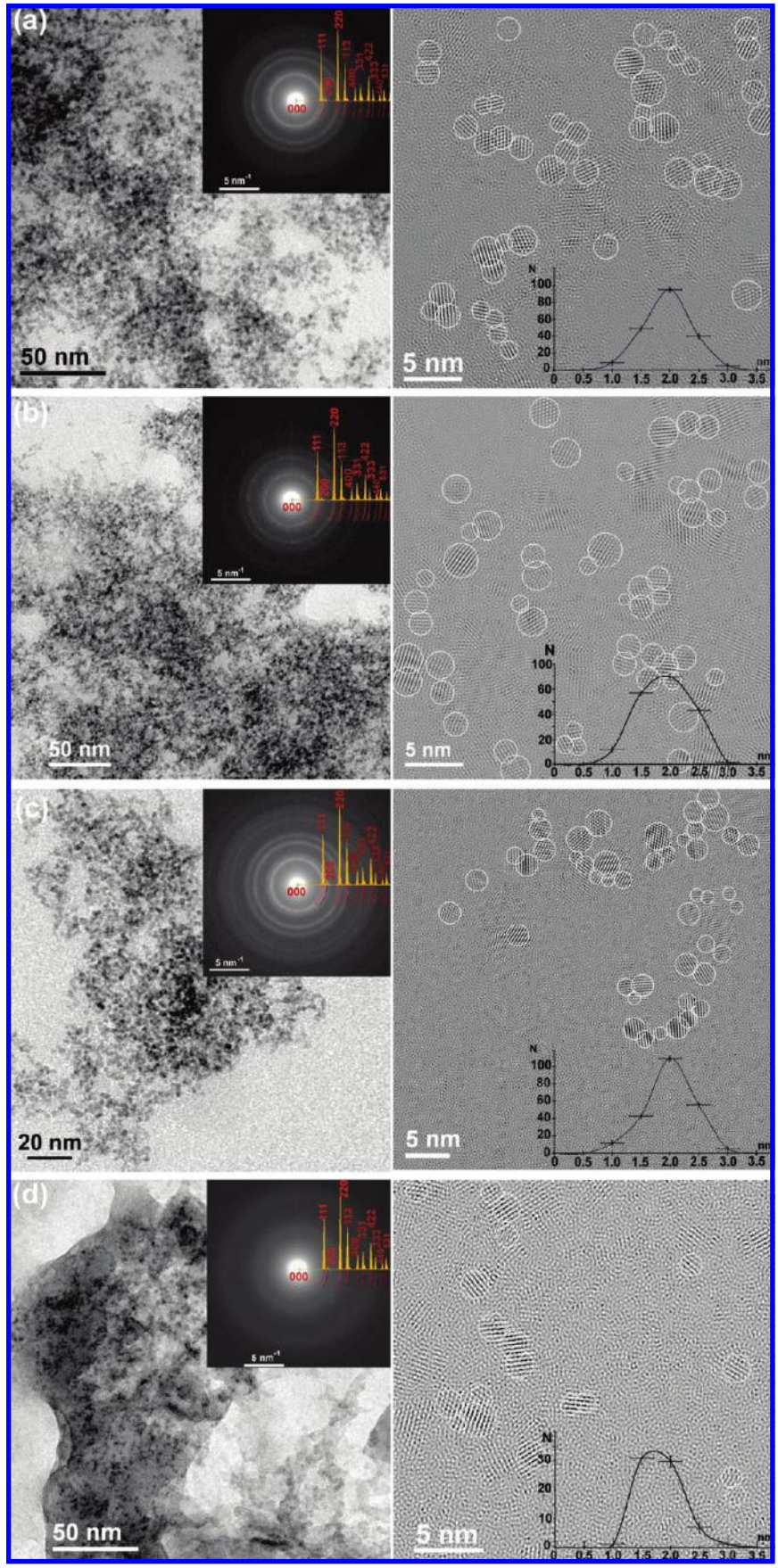

FIGURE 2. TEM images, electron diffraction patterns, and size distribution of uraninite particles. From left to right: TEM images with SAED patterns (inset) and selection of uraninite particles in Fourier-filtered HRTEM images with histogram (inset) of particle size distribution. Microscopy images are for uranium precipitates produced by (a) *Shewanella* sp. HRCR-2, (b) *A. dehalogenans*, (c) *G. sulfurreducens*, and (d) *D. vulgaris*.

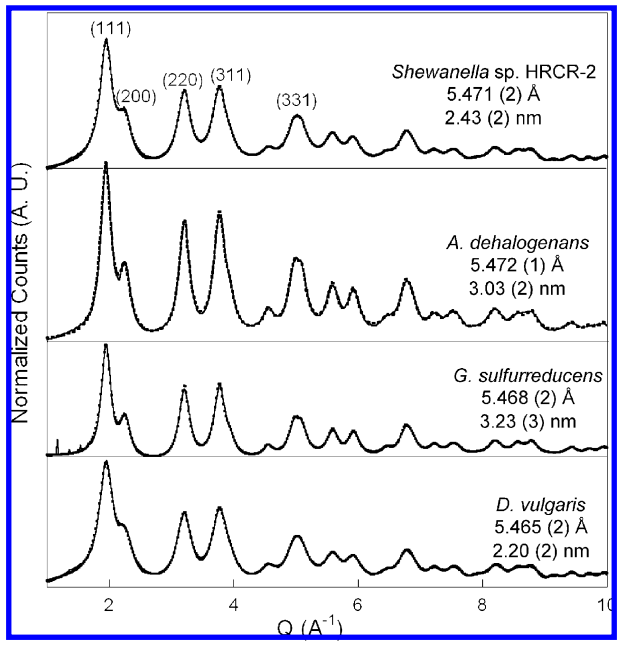

FIGURE 3. Conservation of long-range structure and crystal size between biogenic uraninites. In situ synchrotron powder diffraction (solid line) and Pawley refinements (dashed line) of biogenic uraninites produced by bacteria. Depicted is the calculated lattice parameter (Å) and crystal size (nm) associated with the fits. Miller indices for the associated peaks are labeled on the first pattern.

HCO_3^- buffer to remove residual uranyl, and suspended in Milli-Q prior to structural analysis (*14*).

Protein from a pelleted fraction of the initial incubation (EFPL) was extracted by incubation at 95 °C for 10 min in 0.1% Triton 100-X. After a 100-fold dilution, the protein concentration was determined using the Bradford assay (Biorad, Hercules, CA). At PNNL, protein concentrations were determined using the bicinchoninic acid (BCA) assay (Pierce, Rockford, IL). Frozen 100 μL aliquots of sample were thawed at 95 °C followed by doubling dilutions and the BCA assay.

Electron Microscopy Techniques. TEM samples were prepared by placing a drop of biogenic precipitate suspension on copper/carbon film grids and drying anoxically. Low-dose illumination conditions were used to record the images in order to limit sintering of particles under the electron beam. Further details regarding TEM, high resolution (HRTEM), and ED analyses are given in the Supporting Information.

Synchrotron-Based Analysis. Analysis included X-ray absorption near-edge structure (XANES), extended X-ray absorption fine structure (EXAFS), and synchrotron powder diffraction (SR-PD). Samples were hermetically sealed under an anoxic, nitrogenous atmosphere (2−5% hydrogen) and delivered to SSRL for anoxic processing following published protocols (*14*) which are described in more detail in the Supporting Information.

Results and Discussion

Batch Uranium Removal. In order to conduct intergenus comparisons of uranium removal, strains previously reported to reduce uranium in liquid batch assays were grown under microbe-specific ideal conditions (*1, 3, 4, 14*) and exposed to U(VI) for bioreduction in a geochemically similar environment. The organisms chosen for this study vary in taxonomic order within delta- and gamma-proteobacteria and metabolic activity. Their phylogenetic relationship is shown in Figure SI-1 of the Supporting Information.

For uranium reduction experiments, washed resting cells were incubated with 1000 μM uranyl acetate where the only medium variable was the e^--donor (see Materials and Methods). Characteristic U(VI) removal profiles for three of the bacterial strains are depicted and are representative of time scales, cellular density, and extent of removal for all studied strains (Figure 1). In every case, behavior was characterized by rapid removal of U(VI) with less than 1% of the initial soluble fraction detected after overnight incubations. This removal from solution was accompanied by the formation of a dark-colored precipitate, which was harvested after ~24 h. In contrast, the continued presence of soluble uranium in pasteurized and abiotic controls confirmed a biological role in precipitation.

Characterization of Immobilized Uranium Precipitates by Electron Microscopy. Uranium nanoparticles formed during bacterial incubations were characterized by TEM, EDS, and SAED. Because of the conservation of products and prior publications documenting *Shewanella* (*14, 15*), we focused this analysis at the genus level. Cultures of each of the four genera produced irregularly shaped, extracellular aggregate particles (Figure 2a−d). Fourier filtered HRTEM images were used to determine individual particle size distribution for dispersed particles, and to a lesser extent within aggregates, and revealed strong conservation between genera. As depicted in the insert histograms, compilation of identified particles revealed the following averages and standard deviations of particle size: *Shewanella* sp. HRCR-2, 1.96 nm ± 0.43; *A. dehalogenans*, 1.91 nm ± 0.45; *G. sulfurreducens*, 2.00 nm ± 0.43; and *D. vulgaris*, 1.83 nm ± 0.37. The identified diameters are smaller than 2.5 nm as reported previously for *S. oneidensis* MR-1 (*14*).

Electron diffraction (Figure 2a−d insets) indicated that the solid-phase product of each genus was consistent with cubic uraninite. These observations complement prior observations of extracellular uraninite aggregates with individual nanometer-sized particles observed for these genera (*2, 3, 5, 23, 24*).

Long-Range Structure of Biogenic Uraninites and Crystal Size. SR-PD was used to quantify unit cell size and lattice strain for biogenic products. Pawley fits of the full SR-PD patterns show that the lattice constants for the samples range from 5.465−5.472 Å (Figure 3). These values bracket the literature value for macrocrystal stoichiometric $UO_{2.0}$ of 5.468 Å (*25*) and thus suggest a near-stoichiometric composition. These results are in agreement with published values for *S. oneidensis* MR-1 prepared under slightly different laboratory conditions (*14*).

Pawley fits to SR-PD data provide analytical estimates of average crystal size ranging from 2.2 to 3.2 nm (Figure 3). Previous SR-PD analyses of uraninite produced by *S. oneidensis* MR-1 indicated a crystal size of 3.3 nm (*14*), which was at the upper range of the crystals reported in this study. SR-PD measures the geometric mean particle size, whereas TEM measurements skew toward frequently observed (modal) particle sizes. Particles often exhibit a log-normal distribution with an asymmetric tail toward a larger particle size. Consequently, as observed in our study, the TEM-measured dimensions are typically smaller than those from SR-PD.

Short- and Intermediate-Range Structures and Oxidation States of Biogenic Uraninites. XANES spectra indicated that the immobilized precipitates were consistent with 100 ± 10% $UO_{2.00}$ for five out of six strains. As described in the Supporting Information, a best fit to XANES demonstrates that the *A. dehalogenans* product contains higher valent U, possibly surface U(V) atoms *(26)*, corresponding to a composition of $UO_{2.075}$ (Figure SI-2 of the Supporting Information).

Uranium L_{III}-edge EXAFS was used to characterize the short-range (<4 Å) and intermediate-range (4−10 Å) structure

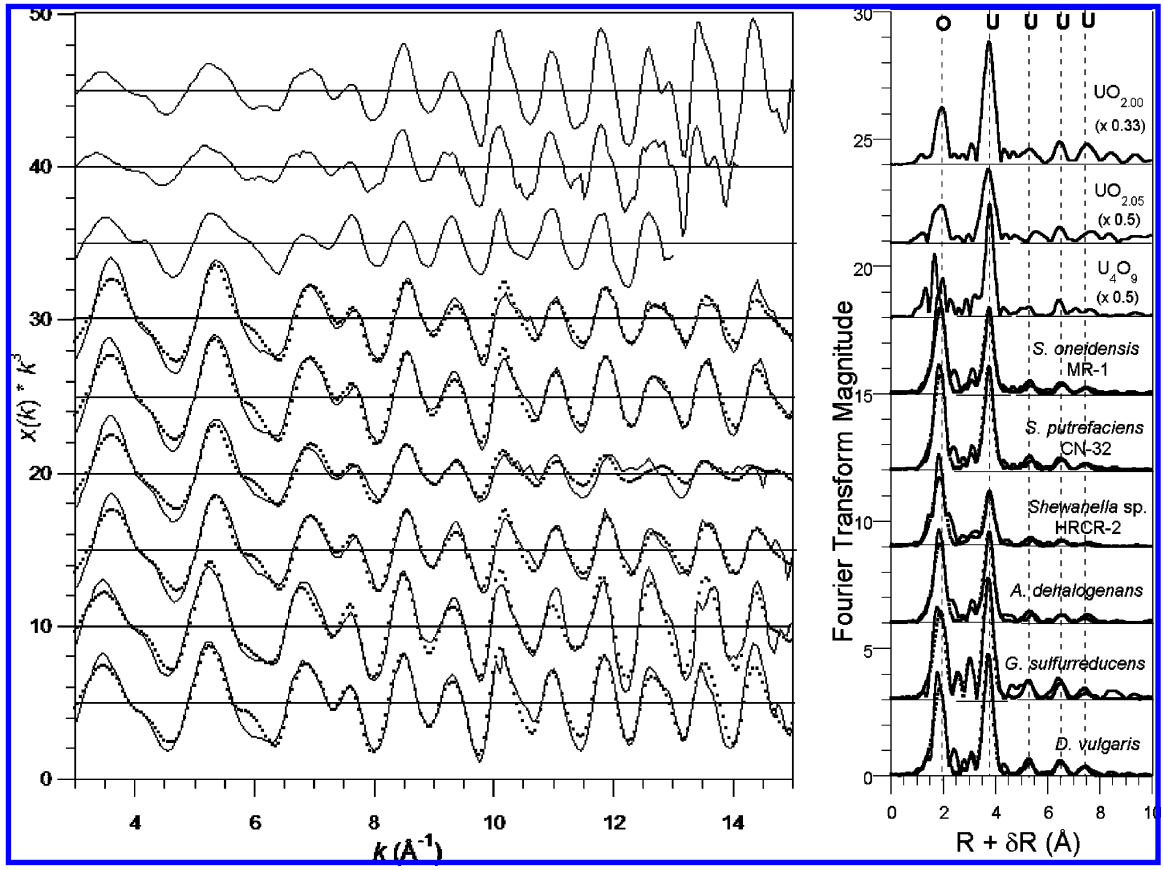

FIGURE 4. EXAFS characterization of immobilized uranium produced by different genera (a) EXAFS spectra (solid line) collected at 77 K with fit to data (dashed line) and (b) corresponding Fourier transform for reduced uranium. Representative spectra for sample UO_{2+x} ($x = 0$, 0.05, and 0.25) are presented as the top three spectra (*11, 14*).

of the reduced uranium precipitates (Figure 4). All spectra show general details expected for uraninite, most notably an O shell at 2.35−2.37 Å (Table 1) and a U shell at 3.86 Å (corresponding to the FT peaks at 1.8 and 3.8 Å, R + δR). In addition to these features, FT peaks are present in the sample data for $R > 4$ Å (terminating at about 8 Å), indicating the presence of significant intermediate-range order.

These results are generally consistent with previous reports of "nano-uraninite" production by different bacteria, while providing a more comprehensive analysis of the products. For example, both *S. oneidensis* MR-1 and *Desulfosporosinius* sp. have been documented to form nanoparticulate (~3 nm) uraninite (*14, 27*). Inoculation of groundwater amended with *G. metallireducens*, a close relative of *G. sulfurreducens*, results in a uranium precipitate with wide XRD spectra indicative of nanoparticles (*2*), and TEM images clearly show irregular nanouranium aggregates formed by *A. dehalogenans* (*24*).

EXAFS spectra were fit (Figure 4, Table 1) to extract quantitative structural details using the model previously described (*14*). Selected key details of the fits are as follows.

O Shell. EXAFS spectra are best fit with one O shell at 2.35−2.37 Å; however, the corresponding FT peak is visually asymmetric in some samples (e.g., *S. oneidensis* and *D. vulgaris*) suggesting the presence of multiple U−O subshells as occurs in UO_{2+x} (*11*). Fits were attempted using two O shells or a single anharmonic Debye−Waller factor; however, these alternate fits did not result in a significant improvement in the model as determined by Hamilton testing (*28*). The sample FTs can be qualitatively compared to those for UO_{2+x}, which exhibit increasing O shell complexity and distortion as x increases from 0 to 0.25. The distortion in our sample spectra is qualitatively less than that observed for $UO_{2.05}$ (Figure 4). When coupled to unit cell parameters that are close to the value for stoichiometric $UO_{2.00}$ (Figure 3), these results suggest that the range of sample compositions is limited to between $UO_{2.00}$ and $UO_{2.05}$. This result is consistent with the XANES findings that the stoichiometry is from 2.00 to 2.075 (±0.025) (Figure SI-2 of the Supporting Information).

U Shell at 3.8 Å. A reduction in the expected coordination number (CN) for this shell is observed (CN = 5.7−6.4) as compared to the bulk value of 12. This under-coordination is consistent with the nanoparticulate size and consequential high proportion of surface-exposed atoms (*13, 14*).

Extended Shells. $UO_{2.0}$ displays FT peaks to at least 10 Å. The absence of FT peaks at >8 Å in the biogenic uraninites (Figure 4) qualitatively suggests that the highly ordered interior portions of the nanoparticles have diameters smaller than the overall particle size. An EXAFS model was applied to quantify the length-scale over which structural order is maintained in the interior of the particles (*14*). The corresponding fit parameter is the EXAFS structural coherence length (SCL), which ranges from 0.9−1.5 nm for different bacteria (Table 1). Comparison of SCL values to overall particle diameters suggests an ordered interior surrounded by a less-ordered rind as observed previously for *S. oneidensis* (*14*).

The EXAFS results for the samples were similar to one another (Figure 4, Table 1). However, the presence of small but significant FT peaks at about 2.6 and 3.0 Å (R + δR) in the *G. sulfurreducens* product indicates the presence of U(IV)−organic (e.g., carboxylate or phophoryl groups (*29*)) or U(IV)−metal moieties. Fits to these peaks using C or P (at about 3.1 and 3.34 Å) were inadequate unless the majority of U(IV) was allowed to be chelated by biomass, which is in direct contradiction to the prominent uraninite U−U signatures in the spectrum and FT for this sample. Using Fe atoms at 2.98 and 3.16 Å as a proxy for first row transition

metals, we achieved a more satisfactory fit but cannot readily account for the origin of this metal from the incubation conditions. In any case, these results imply a stronger association of *G. sulfurreducens* uraninite with metals as adsorbed or structurally incorporated species (*30*), when compared to the other bacteria.

Implications for Environmental Uranium Immobilization. Diverse bacterial strains were found to produce similar nanoparticulate uraninites with particle diameters of 2−3 nm (Figure 3), indicating that in this regard, DMRB and DSRB generate analogous U(IV) oxides. Structural similarity of the products also transcends researcher variability as these analogous uraninites were produced at different laboratories as explained in the methods.These observations lead to the conclusion that for the reported laboratory conditions, phylogenetic and metabolic variability within delta- and gamma-proteobacteria has little effect on the structure and composition of biogenic uraninites. It is important to note that while a trend was not observed across the suite of analysis techniques used in this study, subtle variations in uraninite composition were observed for *Anaeromyxobacter* and *Geobacter* by XANES and EXAFS analysis respectively (Figure 4, Figure SI-2 of the Supporting Information, and Table 1).

As a whole, the biouraninites in our current study are similar to those previously reported for *S. oneidensis* MR-1, which was found to have solubility and surface area normalized dissolution rates similar to chemogenic $UO_{2.0}$ (*10, 14, 26*). As such, it provides justification for geochemical models for bacterial products based on a single set of rate and thermodynamic constants *(26, 30)*.

However, variations in the sizes of biogenic uraninites, with average diameters ranging from 2−5 nm, have been reported (*14, 16, 24*). Because size directly impacts overall dissolution rates, such variability could influence the stability of these biogenic products where larger nanoparticles are more recalcitrant (*31*). Our observation of a conservation of particle size between interspecies products formed under nearly identical conditions suggests that formation diameter may have more to do with geochemical factors than with biological variability. Possible experimental variables identified by contrasting this work with others include initial uranyl concentration, reduction rate, e^--donor, resting cellular density, headspace gas, and buffer composition (*14, 16, 24, 31*). It is however important to emphasize that our work demonstrates that differences in e^--donor and bacteria appear to have minimal effects on uraninite size.

Similarly, the observation that the solid-phase reduction products are independent of phylogeny and electron-donor suggests that nucleation and polymerization of U(IV) may transcend the enzymatic diversity involved in catalyzing these reactions. A possible explanation is that the kinetics of nanoparticulate growth are controlled by a slow abiotic step and that enzymatic U(VI) reduction is relatively fast. Alternatively, biochemical and mutational studies to isolate uranyl reductases with members of the *Desulfovibrio, Geobacter*, and *Shewanella* genera demonstrate that multiheme *c*-type cytochromes function directly in U(VI) reduction (*23, 32*−*36*). Although little amino acid homology exists among this class of proteins, electron transfer through these types of proteins may ultimately influence nanoparticle size and uraninite crystal structure.

The conservation of uraninite structure across these phylogenetically and metabolically distinct cultures suggests that the type of organism and substrate additions may not be critical variables in assessing the success of a reductive immobilization strategy (as quantified by uraninite structure and size). If these results are found to transcend delta- and gamma-proteobacteria, then field-relevant variables such as uranium concentration, groundwater composition, biologically enhanced adsorption-driven reactions, and the potential for redox cycling by iron oxide phases such as green rust, goethite, reduced quinones, or humics *(13, 22, 37)* could play a more important role.

Acknowledgments

Work was funded by Swiss NSF Grants 20021-113784 (RBL&HV), IZK0Z2-123550 (JS), and U.S. DOE-OBER DE-FG02-06ER64227 (RBL&JS) and SCW0041 (ES&JB). Work at PNNL was supported by the Environmental Remediation Sciences Program (ERSP). Battelle Memorial Institute operates PNNL for the DOE under Contract DE-AC05-76RL01830. SSRL is a U.S. national user facility operated by Stanford University on behalf of the U.S. DOE-OBES. Portions of this project were supported by the DOE-BER and NIH-NCRR-funded SSRL Structural Molecular Biology Program. We acknowledge CIME (EPFL) for the use of HRTEM and staff assistance. Assistance was supplied by Pilar Junier (EPFL) who aided in phylogenetic analysis and Yuri Gorby (JCVI) for advice on *Geobacter* growth. Kai Ulrich and Dan Giammar (WUStL) contributed to research development and editing throughout the process. Joe Rogers and Carol Morris provided technical assistance with sample handling and analysis. We thank three anonymous reviewers for their constructive comments.

Supporting Information Available

Additional details regarding experimental methods, phylogenetic relationship of organisms (Figure SI-1), and XANES analysis of biogenic uraninites (SI Results, Figure SI-2). This material is available free of charge via the Internet at http://pubs.acs.org.

Literature Cited

(1) Lovley, D. R.; Phillips, E. J. P.; Gorby, Y. A.; Landa, E. R. Microbial reduction of uranium. *Nature* **1991**, *350* (6317), 413–416.
(2) Gorby, Y. A.; Lovley, D. R. Enzymatic uranium precipitation. *Environ. Sci. Technol.* **1992**, *26* (1), 205–207.
(3) Lovley, D. R.; Phillips, E. J. P. Reduction of uranium by *Desulfovibrio desulfuricans*. *Appl. Environ. Microbiol.* **1992**, *58*, 850–856.
(4) Wu, Q.; Sanford, R. A.; Loffler, F. E. Uranium(VI) reduction by *Anaeromyxobacter dehalogenans* strain 2CP-C. *Appl. Environ. Microbiol.* **2006**, *72* (5), 3608–3614.
(5) Liu, C. X.; Gorby, Y. A.; Zachara, J. M.; Fredrickson, J. K.; Brown, C. F. Reduction kinetics of Fe(III), Co(III), U(VI) Cr(VI), and Tc(VII) in cultures of dissimilatory metal-reducing bacteria. *Biotechnol. Bioeng.* **2002**, *80* (6), 637–649.
(6) Gu, B. H.; Wu, W. M.; Ginder-Vogel, M. A.; Yan, H.; Fields, M. W.; Zhou, J.; Fendorf, S.; Criddle, C. S.; Jardine, P. M. Bioreduction of uranium in a contaminated soil column. *Environ. Sci. Technol.* **2005**, *39* (13), 4841–4847.
(7) Moon, H. S.; Komlos, J.; Jaffe, P. R. Uranium reoxidation in previously bioreduced sediment by dissolved oxygen and nitrate. *Environ. Sci. Technol.* **2007**, *41* (13), 4587–92.
(8) Wu, W. M.; Carley, J.; Luo, J.; Ginder-Vogel, M. A.; Cardenas, E.; Leigh, M. B.; Hwang, C. C.; Kelly, S. D.; Ruan, C. M.; Wu, L. Y.; Van Nostrand, J.; Gentry, T.; Lowe, K.; Mehlhorn, T.; Carroll, S.; Luo, W. S.; Fields, M. W.; Gu, B. H.; Watson, D.; Kemner, K. M.; Marsh, T.; Tiedje, J.; Zhou, J. Z.; Fendorf, S.; Kitanidis, P. K.; Jardine, P. M.; Criddle, C. S. In situ bioreduction of uranium (VI) to submicromolar levels and reoxidation by dissolved oxygen. *Environ. Sci. Technol.* **2007**, *41* (16), 5716–5723.
(9) Anderson, R. T.; Vrionis, H. A.; Ortiz-Bernad, I.; Resch, C. T.; Long, P. E.; Dayvault, R.; Karp, K.; Marutzky, S.; Metzler, D. R.; Peacock, A.; White, D. C.; Lowe, M.; Lovley, D. R. Stimulating the in situ activity of *Geobacter* species to remove uranium from the groundwater of a uranium-contaminated aquifer. *Appl. Environ. Microbiol.* **2003**, *69* (10), 5884–5891.
(10) Ulrich, K. U.; Singh, A.; Schofield, E. J.; Bargar, J. R.; Veeramani, H.; Sharp, J. O.; Bernier-Latmani, R.; Giammar, D. E. Dissolution of biogenic and synthetic UO_2 under varied reducing conditions. *Environ. Sci. Technol.* **2008**, *42* (15), 5600–5606.
(11) Conradson, S. D.; Manara, D.; Wastin, F.; Clark, D. L.; Lander, G. H.; Morales, L. A.; Rebizant, J.; Rondinella, V. Local structure and charge distribution of the $UO_2-U_4O_9$ system. *Inorg. Chem.* **2004**, *43*, 6922–6935.

(12) Janeczek, J.; Ewing, R. C. Structural formula of uraninite. *J. Nucl. Mater.* **1992**, *190*, 128–132.
(13) O'Loughlin, E. J.; Kelly, S. D.; Cook, R. E.; Csencsits, R.; Kemner, K. M. Reduction of uranium(VI) by mixed iron(II)/iron(III) hydroxide (green rust): Formation of UO_2 nanoparticles. *Environ. Sci. Technol.* **2003**, *37* (4), 721–7.
(14) Schofield, E. J.; Veeramani, H.; Sharp, J. O.; Suvorova, E.; Bernier-Latmani, R.; Mehta, A.; Stahlman, J.; Webb, S. M.; Clark, D. L.; Conradson, S. D.; Ilton, E. S.; Bargar, J. R. Structure of biogenic UO_2 produced by *Shewanella oneidensis* MR-1. *Environ. Sci. Technol.* **2008**, *42* (21), 7898–7905.
(15) Singer, D. M.; Farges, F.; Brown, G. E. Biogenic nanoparticulate UO_2: Synthesis, characterization, and factors affecting surface reactivity. *Geochim. Cosmochim. Acta* **2009**, *73* (12), 3593–3611.
(16) Burgos, W. D.; McDonough, J. T.; Senko, J. M.; Zhang, G.; Dohnalkova, A. C.; Kelly, S. D.; Gorby, Y. A.; Kemner, K. M. Characterization of uraninite nanoparticles produced by *Shewanella oneidensis* MR-1. *Geochim. Cosmochim. Acta* **2008**, *72* (20), 4901–4915.
(17) Cardenas, E.; Wu, W. M.; Leigh, M. B.; Carley, J.; Carroll, S.; Gentry, T.; Luo, J.; Watson, D.; Gu, B.; Ginder-Vogel, M.; Kitanidis, P. K.; Jardine, P. M.; Zhou, J.; Criddle, C. S.; Marsh, T. L.; Tiedje, J. A. Microbial communities in contaminated sediments, associated with bioremediation of uranium to submicromolar levels. *Appl. Environ. Microbiol.* **2008**, *74* (12), 3718–3729.
(18) Vrionis, H. A.; Anderson, R. T.; Ortiz-Bernad, I.; O'Neill, K. R.; Resch, C. T.; Peacock, A. D.; Dayvault, R.; White, D. C.; Long, P. E.; Lovley, D. R. Microbiological and geochemical heterogeneity in an in situ uranium bioremediation field site. *Appl. Environ. Microbiol.* **2005**, *71* (10), 6308–6318.
(19) Brodie, E. L.; DeSantis, T. Z.; Joyner, D. C.; Baek, S. M.; Larsen, J. T.; Andersen, G. L.; Hazen, T. C.; Richardson, P. M.; Herman, D. J.; Tokunaga, T. K.; Wan, J. M.; Firestone, M. K. Application of a high-density oligonucleotide microarray approach to study bacterial population dynamics during uranium reduction and reoxidation. *Appl. Environ. Microbiol.* **2006**, *72* (9), 6288–6298.
(20) Holmes, D. E.; Finneran, K. T.; O'Neil, R.; Lovley, D. R. Enrichment of members of the family *Geobacteraceae* associated with stimulation of dissimilatory metal reduction in uranium-contaminated aquifer sediments. *Appl. Environ. Microbiol.* **2002**, *68* (5), 2300–2306.
(21) Suzuki, Y.; Kelly, S. D.; Kemner, K. M.; Banfield, J. F. Microbial populations stimulated for hexavalent uranium reduction in uranium mine sediment. *Appl. Environ. Microbiol.* **2003**, *69* (3), 1337–1346.
(22) N'Guessan, A. L.; Vrionis, H. A.; Resch, C. T.; Long, P. E.; Lovley, D. R. Sustained removal of uranium from contaminated groundwater following stimulation of dissimilatory metal reduction. *Environ. Sci. Technol.* **2008**, *42* (8), 2999–3004.
(23) Marshall, M. J.; Beliaev, A. S.; Dohnalkova, A. C.; Kennedy, D. W.; Shi, L.; Wang, Z.; Boyanov, M. I.; Lai, B.; Kemner, K. M.; McLean, J. S.; Reed, S. B.; Culley, D. E.; Bailey, V. L.; Simonson, C. J.; Saffarani, D. A.; Romine, M. F.; Zachara, J. M.; Fredrickson, J. K. *c*-Type cytochrome-dependent formation of U(IV) nanoparticles by *Shewanella oneidensis*. *PLoS Bio.* **2006**, *4* (8), 1324–1333.
(24) Marshall, M. J.; Dohnalkova, A. C.; Kennedy, D. W.; Plymale, A. E.; Thomas, S. H.; Löffler, F. E.; Sanford, R. A.; Zachara, J. M.; Fredrickson, J. K.; Beliaev, A. S. Electron donor-dependent radionuclide reduction and nanoparticle formation by *Anaeromyxobacter dehalogenans* strain 2CP-C. *Environ. Microbiol.* **2008**, *11* (2), 534–543.
(25) Wyckoff, R. W. G. *Crystal Structures*. John Wiley & Sons: New York, 1978; Vol. 2.
(26) Ulrich, K.-U.; Ilton, E.; Veeramani, H.; Sharp, J. O.; Bernier-Latmani, R.; Schofield, E. J.; Bargar, J. R.; Giammar, D. E. Comparitive dissolution kinetics of biogenic and chemogenic uraninite under oxidizing conditions in the presence of carbonate. *Geochim. Cosmochim. Acta* **2009**, *73* (20), 6065−6083.
(27) Suzuki, Y.; Kelly, S. D.; Kemner, K. M.; Banfield, J. F. Nanometre-size products of uranium bioreduction. *Nature* **2002**, *419* (6903), 134–135.
(28) Hamilton, W. C. Significance tests on the crystallographic *R* factor. *Acta Crystallogr.* **1965**, *18*, 502.
(29) Kelly, S. D.; Kemner, K. M.; Carley, J.; Criddle, C.; Jardine, P. M.; Marsh, T. L.; Phillips, D.; Watson, D.; Wu, W.-M. Speciation of uranium in sediments before and after in situ biostimulation. *Environ. Sci. Technol.* **2008**, *42* (5), 1558–1564.
(30) Veeramani, H.; Schofield, E.; Sharp, J. O.; Suvorova, E.; Ulrich, K. U.; Mehta, A.; Giammar, D. E.; Bargar, J. R.; Bernier-Latmani, R. Effect of Mn(II) on the structure and reactivity of biogenic UO_2. *Environ. Sci. Technol.* **2009**, *43* (17), 6541−6547.
(31) Senko, J. M.; Kelly, S. D.; Dohnalkova, A. C.; McDonough, J. T.; Kemner, K. M.; Burgos, W. D. The effect of U(VI) bioreduction kinetics on subsequent reoxidation of biogenic U(IV). *Geochim. Cosmochim. Acta* **2007**, *71* (19), 4644–4654.
(32) Lovley, D. R.; Widman, P. K.; Woodward, J. C.; Phillips, E. J. P. Reduction of uranium by cytochrome c_3 of *Desulfovibrio vulgaris*. *Appl. Environ. Microbiol.* **1993**, *59* (11), 3572–3576.
(33) Payne, R. B.; Gentry, D. M.; Rapp-Giles, B. J.; Casalot, l.; Wall, J. D. Uranium reduction by *Desulfovibrio desulfuricans* strain G20 and a cytochrome c_3 mutant. *Appl. Environ. Microbiol.* **2002**, *68* (6), 3129–3132.
(34) Lloyd, J. R.; Leang, C.; Myerson, A. L. H.; Coppi, M. V.; Cuifo, S.; Methe, B.; Sandler, S. J.; Lovley, D. R. Biochemical and genetic characterization of PpcA, a periplasmic *c*-type cytochrome in *Geobacter sulfurreducens*. *Biochem. J.* **2003**, *369*, 153–161.
(35) Shelobolina, E. S.; Coppi, M. V.; Korenevsky, A. A.; DiDonato, L. N.; Sullivan, S. A.; Konishi, H.; Xu, H. F.; Leang, C.; Butler, J. E.; Kim, B. C.; Lovley, D. R. Importance of *c*-type cytochromes for U(VI) reduction by *Geobacter sulfurreducens*. *BMC Microbiol.* **2007**, *7*, 16.
(36) Bencheikh-Latmani, R.; Williams, S. M.; Haucke, L.; Criddle, C. S.; Wu, L.; Zhou, J.; Tebo, B. M. Global transcriptional profiling of *Shewanella oneidensis* MR-1 during Cr(VI) and U(VI) reduction. *Appl. Environ. Microbiol.* **2005**, *71* (11), 7453–7460.
(37) Fredrickson, J. K.; Zachara, J. M.; Kennedy, D. W.; Duff, M. C.; Gorby, Y. A.; Li, S. M. W.; Krupka, K. M. Reduction of U(VI) in goethite (α-FeOOH) suspensions by a dissimilatory metal-reducing bacterium. *Geochim. Cosmochim. Acta* **2000**, *64* (18), 3085–3098.

ES901281E